Bull Earthquake Eng (2007) 5:571–589
DOI 10.1007/s10518-007-9047-0

ORIGINAL RESEARCH PAPER

Centrifuge modeling of seismic response of layered soft clay

M. H. T. Rayhani · M. H. El Naggar

Received: 27 November 2006 / Accepted: 28 July 2007 / Published online: 7 September 2007

Abstract Centrifuge modeling is a valuable tool used to study the response of geotechnical structures to infrequent or extreme events such as earthquakes. A series of centrifuge model tests was conducted at 80*g* using an electro-hydraulic earthquake simulator mounted on the C-CORE geotechnical centrifuge to study the dynamic response of soft soils and seismic soil–structure interaction (SSI). The acceleration records at different locations within the soil bed and at its surface along with the settlement records at the surface were used to analyze the soft soil seismic response. In addition, the records of acceleration at the surface of a foundation model partially embedded in the soil were used to investigate the seismic SSI. Centrifuge data was used to evaluate the variation of shear modulus and damping ratio with shear strain amplitude and confining pressure, and to assess their effects on site response. Site response analysis using the measured shear wave velocity, estimated modulus reduction and damping ratio as input parameters produced good agreement with the measured site response. A spectral analysis of the results showed that the stiffness of the soil deposits had a significant effect on the characteristics of the input motions and the overall behavior of the structure. The peak surface acceleration measured in the centrifuge was significantly amplified, especially for low amplitude base acceleration. The amplification of the earthquake shaking as well as the frequency of the response spectra decreased with increasing earthquake intensity. The results clearly demonstrate that the layering system has to be considered, and not just the average shear wave velocity, when evaluating the local site effects.

Keywords Seismic response · Soil–structure interaction · Soft clay · Centrifuge modeling

M. H. T. Rayhani (✉) · M. H. El Naggar
Department of Civil and Environmental Engineering, University of Western Ontario,
London, ON N6A 5B9, Canada
e-mail: mtofighr@uwo.ca

M. H. El Naggar
e-mail: helnaggar@eng.uwo.ca

1 Introduction

The study of modern geotechnical earthquakes recognizes the strong influence of local site effects on the intensity and frequency content of input motion in structures. Recent destructive earthquakes including the 1985 Michoacan Earthquake, the 1989 Loma Prieta Earthquake, the 1994 Northridge Earthquake, and the 1995 Kobe Earthquake revealed the role of local site conditions in modifying and changing the characteristics of the strong ground motion. More recently, the observed response of soft soil profiles during the 1999 Izmit Earthquake indicated the possibility of significant ground amplification. Local site effects can cause substantially different amounts of structural damage in the same general area, but in general, softer geologic conditions may cause larger amplification of the seismic waves. Therefore, understanding the effects of local site conditions on the strong ground motion is of particular importance for the mitigation of earthquake disasters as well as future earthquake resistant design.

Seismic site response analysis has been studied extensively over the last few decades. However, available data regarding the dynamic properties and response of soft clay soils subjected to strong seismic shaking has been limited.Tiers and Seed (1968) studied the effect of strain level and load cycles on the parameters of the hyperbola model with San Francisco Bay mud. Hardin and Drnevich (1972) carried out a large number of tests and presented empirical equations to evaluate the dynamic modulus and damping ratio of soft clay. Vucetic and Dobry (1991) proposed that the plasticity index (*PI*) was the key factor influencing the dynamic modulus and damping ratio of both normally consolidated and over consolidated soils. The normalized dynamic modulus increased and the damping ratio decreased with an increase of *PI*. Lanzo et al. (1997) studied the trend of the dynamic modulus and damping ratio under small strains through cyclic simple shear test.

Centrifuge modeling is effective in evaluating the site response characteristics of soft soils. One advantage of centrifuge modeling is that it allows a physical parameter study to be performed allowing the effects of parameters such as strata thickness, soil properties, earthquake frequency content, and level of shaking to be observed. The results of experimental parameter studies are useful in verifying and validating numerical methods for site response analysis. Elgamal et al. (2005) studied the dynamic shear modulus and damping of saturated Nevada sand using centrifuge tests and numerical simulation.

Further research is still required to estimate the amplification/attenuation of shallow soft deposits. Long-term needs include obtaining strong motion records of earthquake shaking at fully characterized sites, and site response analyses that compare predicted and recorded motions to assess the predictive capabilities of analysis methods. Such soft soil studies are of significance for many urban earthquake prone areas worldwide.

2 Objective and scope of work

The objective of the research described in this paper is to evaluate the seismic behavior of soft to medium stiff clay soils. Centrifuge seismic testing of soft soil deposits was performed using a geotechnical centrifuge at the C-CORE testing facilities in Newfoundland. The amplification of the earthquake motion through different soil profiles while considering different excitation levels and frequency contents was analyzed with special emphasis on seismic soil–structure interaction.

Table 1 Index properties of glyben samples

Liquid limit	Plastic limit	Plasticity index	Specific gravity	Dry density (kg/m^3)	Glycerin content (%)	Void ratio
50	39.5	10.5	2.73	1770	39	0.94

Table 2 G_{max} for glyben with different confining pressures from resonant column tests

Sample	Description	G_{max} (MPa)				
		σ_c 30 kPa	σ_c 60 kPa	σ_c 90 kPa	σ_c 150 kPa	σ_c 300 kPa
GLY45	Soft clay	3	3.2	3.7	4.2	5
GLY40	Stiff clay	8.5	10	11.5	14	15

3 Soil properties

An artificial clay known as "glyben" was used in the present research. It is a mixture of sodium bentonite powder and glycerin. The mix proportions are varied to achieve shear strengths in the range of 5–100 kPa. Glyben exhibits constant shear strength behavior as verified by undrained triaxial tests conducted by Mayfield (1963). Kenny and Andrawes (1997) demonstrated in a large number of undrained triaxial tests and vane shear tests that glyben behaves generally as a $\phi_u = 0$ material under quick undrained loading. It has several advantages as a laboratory material including: (i) different strengths that are obtained by varying the proportions of bentonite and glycerin; (ii) complete insensitivity to handling; and (iii) negligible evaporation of glycerin at room temperature. Disadvantages of glyben are that pore-water pressure measurements are precluded and samples cannot be consolidated from slurry and must be formed by compaction.

Table 1 presents the physical properties of optimum compaction glyben clay (Rayhani and El Naggar 2007). The glyben properties are listed in Table 1. It is noted that these properties lie within the range for soft clay soil (however, based on glycerin not water content). The mean vane shear strength was approximately 30 kPa and 60 kPa for soft and medium stiff glyben, respectively. Table 2 illustrates maximum shear modulus for glyben with 40% and 45% glycerin ratios from resonant column tests (Rayhani and El Naggar 2007). Similar to normally consolidated clay behavior, the shear moduli at low strain increased with confining pressure for both soils.

Glyben clay with glycerin ratios of 45% and 40% and undrained vane shear strengths of about 30 kPa and 60 kPa, respectively, was used here to simulate soft and medium stiff clay behavior in model tests. The density of glyben with 45% glycerin and 55% bentonite was 1,575 kg/m^3 and its voids ratio is e = 1.36. The density and void ratio for clay with 40% glycerin were 1,593 kg/m^3 and 1.21, respectively.

4 Centrifuge modeling

Centrifuge model tests have been conducted at 80g on the C-CORE 5.5 m radius beam centrifuge located at Memorial University of Newfoundland. An electro-hydraulic earthquake simulator (EQS) was mounted on the centrifuge to apply a one-dimensional prescribed base

Table 3 Vane shear test results during sample preparation

Model Depth (mm)	RG-01Vane shear, S_u (kPa)			RG-02 Vane shear, S_u (kPa)		
Location	Left	Center	Right	Left	Center	Right
50	27	27.5	26.5	29	29.5	30
100	29	29.5	28	30	31	31
150	29.5	30	29	58	57	59
200	31	31.5	30.5	59	59	59.5
250	30	30	29	60	61	61
300	30	31	31.5	60	59.5	60
350	31	32	32	62	62	63

input motion. A model container with inner dimensions of 0.73 m in length, 0.3 m in width, and 0.57 m in height was used to contain the model soil. The centrifuge models comprised a uniform soil profile (RG-01), and a layered soil profile (RG-02). The uniform soil model consisted of soft clay with shear strength of about 30 kPa and the layered model consisted of a lower layer of medium stiff clay ($S_u = 60$ kPa) and an upper layer of soft clay ($S_u = 30$ kPa). The results are presented in prototype units unless otherwise noted.

4.1 Model configuration and preparation

Figure 1 shows the configurations of the uniform and layered soil models. The system models consisted of a rigid structure, soil and a foundation model slightly embedded in the soil. The total thickness of the soil model was approximately 0.375 m, simulating 30 m on a prototype scale. At 80g, the resulting average bearing pressure beneath the structure model was 95 kPa. This arrangement represents a reasonable simulation for the behavior of rectangular 10-storey buildings. The models were instrumented to measure free field and foundation accelerations, free field displacements, and local deformations on basement walls and foundation slabs.

Glycerin and bentonite were mixed at a ratio of 45%/55% for soft clay and 40%/60% for medium stiff clay. The mixture was covered with a plastic wrap after mixing and was allowed to cure for about 2 h. The curing process produced a more even distribution of glycerin throughout the mix. The soil was then deposited in the centrifuge container. The models were prepared by tamping the soil in layers to obtain the desired void ratio (90% of maximum dry density). The homogeneity of each clay layer was checked by conducting vane shear tests at depth intervals of 50 mm. Table 3 presents the vane shear test results for both models at different locations and levels. It is noted from the table that variations of shear strength were less than 5% for each layer, which shows reasonable uniformity in samples.

Ten accelerometers were placed within the soil bed, as shown in Fig. 1, by tamping the clay to the required level, placing the instrument in the desired position and then adding more soil to the required level. Two accelerometers were placed on top of the structure and one was attached to its wall. Linear Variable Differential Transformers (LVDTs) were used to measure the settlement of the soil surface and the vertical displacement of the model structure. To measure the soil settlement, the extenders from the core of LVDTs rested against tin disks, approximately 10 mm in diameter. Once the model preparation was complete, the package was carefully moved onto the centrifuge arm using a forklift. All instrumentations

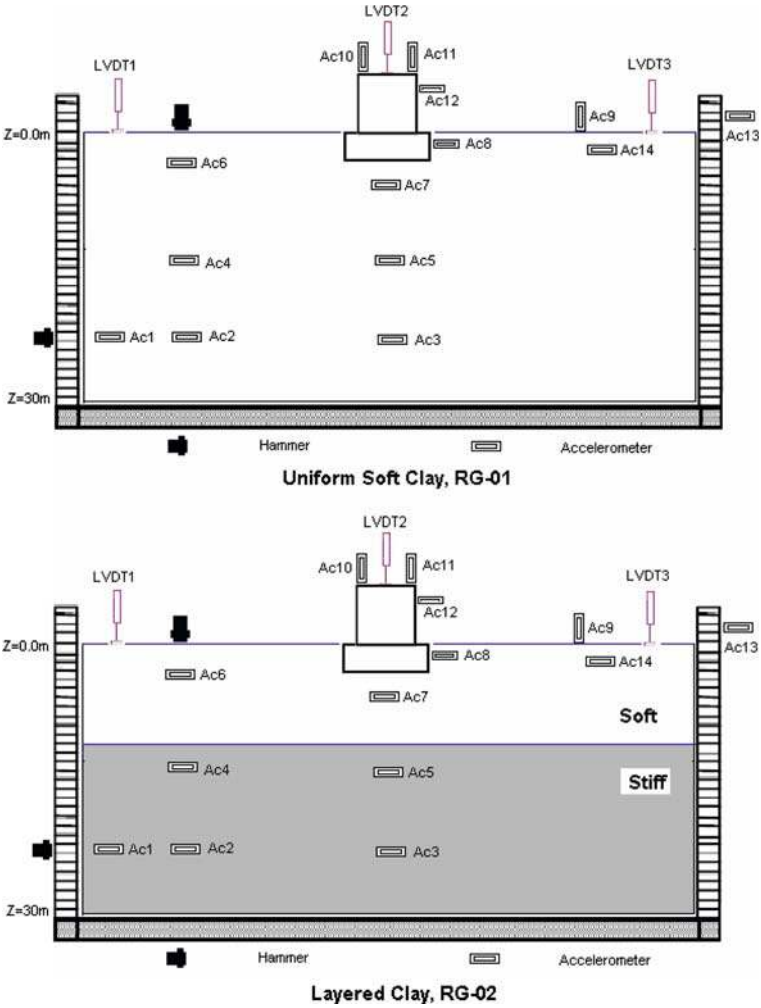

Fig. 1 Centrifuge model configuration in prototype scale

were then connected to the signal box and the model surface profile and the temperature of soil were measured.

4.2 Shear strength profile

T-bar tests were performed at 80g to determine a continuous profile of the deposit undrained shear strength, S_u. The T-bar was 31 mm wide and 7.9 mm in diameter and was pushed into the soil at a rate of approximately 3 mm/s. The results were interpreted using the plasticity solution for the limiting pressure acting on a cylinder moving laterally through purely cohesive soil, which gives the limiting force acting on the cylinder as (Randolf and Houlsby 1984):

$$S_u = \frac{P}{N_b d} \tag{1}$$

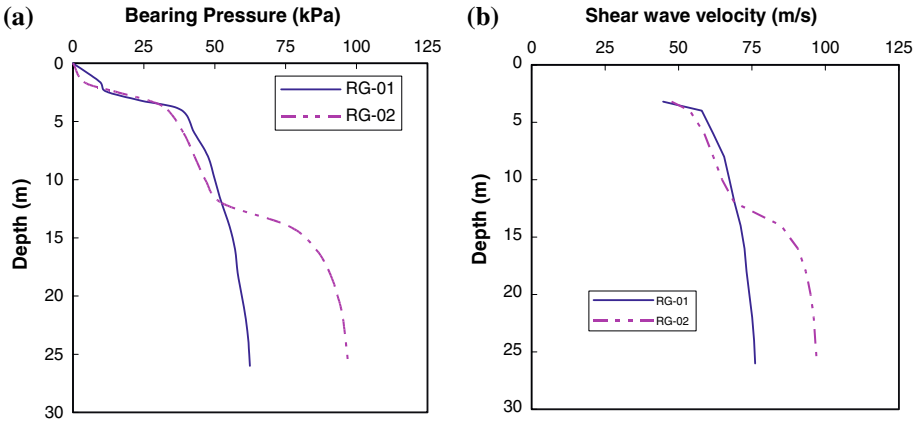

Fig. 2 (**a**) Shear strength versus depth, and (**b**) shear wave velocity profile for both models

where P is force per unit length acting on the cylinder, d is the diameter of cylinder and N_b is the bar factor. The factor N_b of the T-bar was considered equal to 10.5 in the interpretation of the results (Rayhani and El Naggar 2007).

Figure 2a shows the T-bar results in the centrifuge container at $80g$ for both test models. The measured shear strength (using Eq. 1) varied between 40 and 60 kPa in model RG-01 and 40–50 kPa for the upper soft clay and 85–95 kPa for the medium stiff clay in model RG-02. The changes of slopes in top and bottom portions of model are common in T-bar tests, and are attributed to the limitation of the T-bar device (Randolph 2004). Therefore, results at top and bottom might not be reliable. The shear strength increased slightly with depth (i.e., with confining pressure) in both models. The undrained shear strength obtained from the T-bar tests was higher than the shear vane results, which could be due to using different testing techniques, high penetration speed of 3 mm/s for the T-bar and/or difference in stress level between $1g$ in vane tests and $80g$ level in T-bar tests.

4.3 Shear wave velocity

The hammer test was used to evaluate the shear wave velocity for each gravity level in the centrifuge model. The test procedure consisted of striking the steel base plate of the soil container with a sledge hammer which generated compression waves that were detected by the arrays of accelerometers inside the soil. Differential travel times were estimated (using the first strong peak interpretation method) and the compression wave velocity, v_p, was computed once the accelerometer positions were known.

The compression wave velocity, v_p, was evaluated at progressively increasing g-levels from 10 to $80g$. The shear wave velocity, v_s, was estimated based on the p-wave velocity records and the Poisson's ratio of the soil, ν, i.e.,

$$(v_p/v_s) = [(1-\nu)/(0.5-\nu)]^{0.5} \tag{2}$$

The soil Poisson's ratio, $\nu = 0.43$ was obtained based on v_p and v_s measurements in resonant column tests performed on the same glyben mix (Rayhani and El Naggar 2007).

Table 4 shows the shear wave velocity, v_s, of glyben at different centrifuge gravity levels and over a wide range of confining pressures in the soil profile. The equivalent confining pressure for each gravity level was estimated assuming the coefficient of lateral earth pressure,

Table 4 Shear and compression wave velocity of soil in centrifuge container

Centrifuge gravity (g)	σ_c (kPa)	RG-01		RG-02	
		V_p (m/s)	V_s (m/s)	V_p (m/s)	V_s (m/s)
10	35	140	50	190	65
20	70	160	55	220	77
30	106	190	65	275	95
40	142	200	70	290	102
50	177	230	80	320	112
60	213	245	85	340	120
70	248	255	90	360	125
80	283	260	92	370	130

$K_0 = 0.5$ and octahedral confining stress. It is noted from Table 4 that, similar to natural soils, the shear wave velocity increased with an increase in the octahedral confining stress. The measured shear wave velocity in model RG-01 varied between 50 and 90 m/s, with an average of 73 m/s, and in RG-02 varied between 65 and 130 m/s with an average of 100 m/s.

The shear wave velocity of only the lower soil layer was measured from the hammer test. Therefore, the shear wave velocity profile at different depths was also estimated using established relations between shear strength and shear wave velocity for glyben clay (Rayhani and El Naggar 2007). As it can be seen from the Fig. 2b, the shear wave velocity gradually increased with depth in both models. The estimated shear wave velocity was slightly less than those established using the P-wave measurements.

4.4 Shaking events and data set

Each test model was subjected to several earthquake-like shaking events at a centrifugal acceleration level of $80g$. The earthquake motions were applied using the electro-hydraulic simulator described by Coulter and Phillips (2003). Table 5 shows the input excitations, i.e., scaled versions of an artificial western Canada earthquake (Seid-karbasi 2003) and the Port Island ground motion recorded during the 1995 Kobe Earthquake. The model input motions varied from $2.5g$ to $43g$, at target frequencies from 40–200 Hz (simulating prototype earthquakes between $0.03g$ and $0.54g$).

4.5 Testing procedure

The centrifuge speed was increased gradually until a gravity level of $80g$ was reached. Displacement measurements were taken continuously during the swing-up in order to monitor the soil settlement and ensure that the instruments functioned correctly. The earthquake input motions, either A2475 (Western Canada) or Kobe (1995) were applied at $80g$. Four earthquakes of increasing size and different frequency contents were fired in model RG-01, and five earthquakes were fired in model RG-02. The test data was collected using a high-speed data acquisition system.

Table 5 Earthquake input motion in centrifuge tests

Model	Input acceleration	Prototype		Centrifuge test (scale 1:80)	
		Peak Acc. (g)	Dominant freq. (Hz)	Peak Acc. (g)	Dominant freq. (Hz)
RG-01Uniform clay	WCL	0.1	0.93	8	74.5
	WCM	0.2	0.93	16	74.5
	WCH	0.38	0.93	30.5	74.5
	Kobe (1995)	0.54	2.19	43	175
RG-02 Layered clay	WCL	0.1	0.93	8	74.5
	WCM	0.2	0.93	16	74.5
	WCH	0.38	0.93	30.5	74.5
	Kobe (1995)	0.03	2.19	2.5	175
	Kobe (1995)	0.54	2.19	43	175

Table 6 Shaking events and peak accelerations (units in prototype scale)

Model	Base Acc.	RG-01 (g)				RG-02 (g)			
Event ID	(g)	A3	A6	A7	A12	A3	A6	A7	A12
WCL	0.1	0.125	0.15	0.18	0.2	0.12	0.19	0.19	0.28
WCM	0.2	0.19	0.24	0.28	0.33	0.19	0.28	0.275	0.41
WCH	0.38	0.385	0.43	0.51	0.6	0.39	0.4	0.39	0.49
KL	0.03	–	–	–	–	0.04	0.06	0.05	0.08
KH	0.54	0.63	0.61	0.72	1.0	0.61	0.6	0.675	0.87

5 Test results

The testing results are discussed with respect to accelerations and displacements recorded at various depths and locations.

5.1 Accelerations

Table 6 lists peak accelerations at different locations for all shaking events (see Fig. 1): A3 near the base; A6 near the surface; A7 beneath the structure; and A12 on the structure. Peak accelerations generally increased from base to surface. The peak acceleration near the surface in the longitudinal direction ranged from 0.125 to 0.75$g$for model RG-01 and from 0.04g to 0.675g for model RG-02. This range of peak acceleration covered both linear and nonlinear response scenarios. The peak accelerations of the structure were 10–30% greater than the values measured at the soil beneath the structure. The free field accelerations were slightly less than those beneath the structure in model RG-01, but were almost the same in model RG-02.

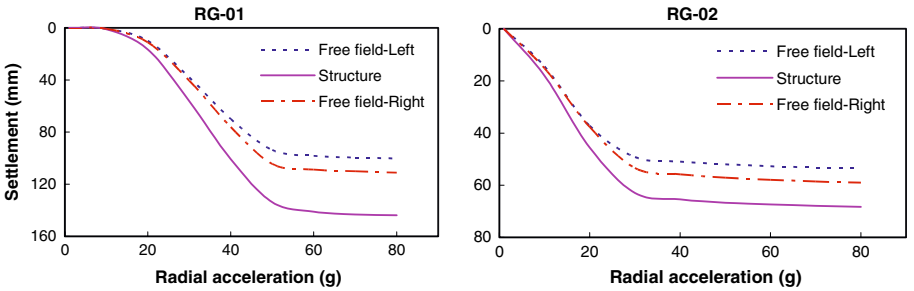

Fig. 3 Settlements curves from 1g to 80g, before earthquake loading

5.2 Settlements

Figure 3 shows the settlement as the gravity field increased from 1g to 80g for both the structure and free field. The maximum settlements for the structure were about 140 and 70 mm, for models RG-01 and RG-02 and were 60 and 110 mm for the free field. Additional settlements of 2–4 mm occurred during earthquake shakings. It is noted that the vast majority of settlement occurred as the model swung up from 1g to about 50g. This initial (almost immediate) settlement is attributed to compaction of glyben. The settlement measured as the model spun at 80g was negligible and was attributed to consolidation. The rate of consolidation, however, is very slow compared to that for natural and artificial clays (e.g., Bransby et al. 2001). This represents a significant saving of centrifuge time as it eliminates the consolidation time required for natural clays.

6 Analysis and discussion

6.1 Shear stress–strain histories

The Shear stress and shear strain response at a particular depth may be obtained using the recorded lateral accelerations, assuming 1D vertically propagating shear waves (Zeghal et al. 1995). The shear stress at any depth was estimated by integrating the equation of an idealized one-dimensional shear beam as:

$$\tau(z,t) = \int_0^z \rho\, \ddot{u}\, dz \tag{3}$$

where z is depth coordinate; τ is horizontal shear stress; ü is horizontal acceleration and ρ is density (Zeghal et al. 1995). Linear interpolation between accelerations was employed to evaluate the shear stress at each level. To calculate the shear strain, displacement records were first obtained through double integration of the corresponding recorded acceleration histories. Acceleration data were band-filtered prior to integration for both velocity and displacement records. Brennan et al. (2005) mentioned the importance of filtering in evaluation of shear strain data from centrifuge test results. The shear strain histories were then evaluated using the displacement data and the spacing between accelerometers. The estimated seismic shear stress and shear strain histories are related by the soil shear stiffness characteristics at each accelerometer level (Zeghal et al. 1995). The shear stress–strain hysteresis are shown in Fig. 4 at depths 3 m, 12 m, and 20 m during WCM shaking event for RG-01 clay model. The WCL event provided a low strain soil response and the slope of the hysteresis loop

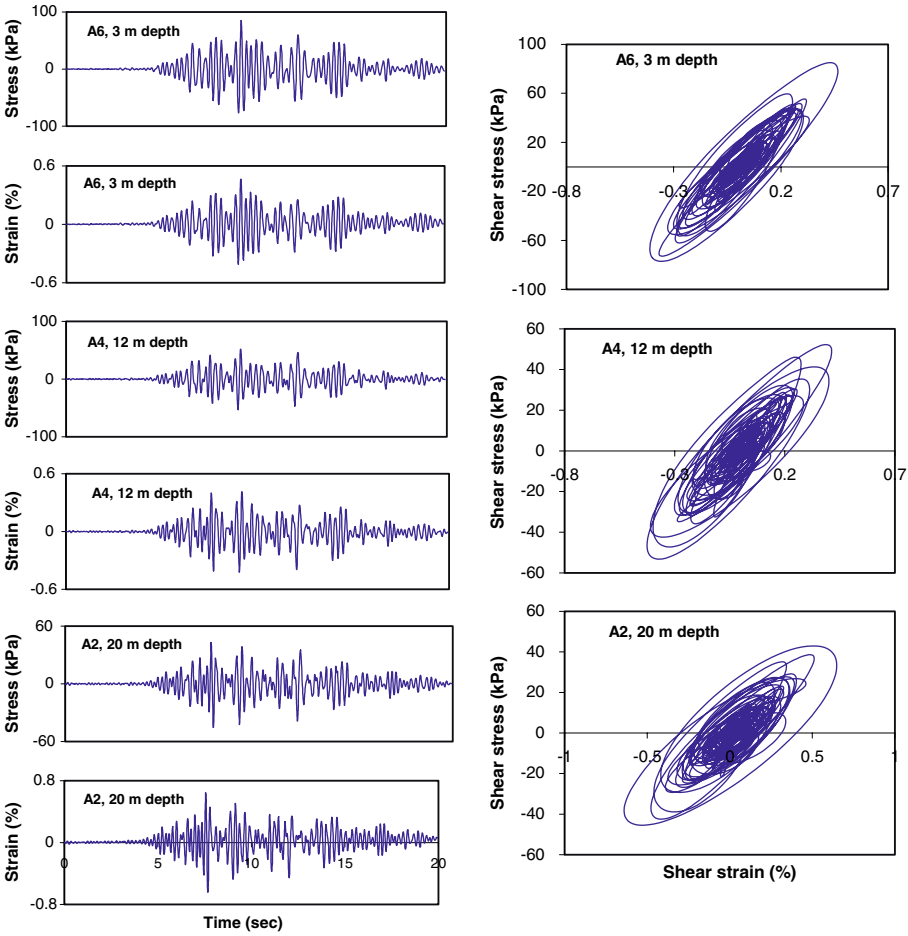

Fig. 4 Shear stress–strain histories at different depths during WCM event, model RG-01

increased with the depth of accelerometer, indicating the effect of confining pressure on soil shear stiffness. The shear strain level increased with applying stronger shaking events to the soil model (WCM and WCH) and the soil shear stiffness, manifested by the hysteresis loop slope, decreased with the strain amplitude. The area of the shear stress–strain curve, and thus the soil damping, increased with strain amplitude and decreased with depth.

6.2 Assessment of shear modulus and damping ratio

The soil shear modulus and equivalent damping ratio were evaluated, as a function of shear strain amplitude, from the stress–strain cycles of the WCL, WCM, and WCH excitations for model RG-01. The soil shear strain during the tests ranged from about 0.1% to 1.0%. The shear modulus was estimated using the secant slope of the representative shear stress–strain loop for each shaking event at 3 m, 12 m, and 20 m depth. The measured shear moduli were normalized by the small-strain shear modulus, G_{max}, established from the hammer test

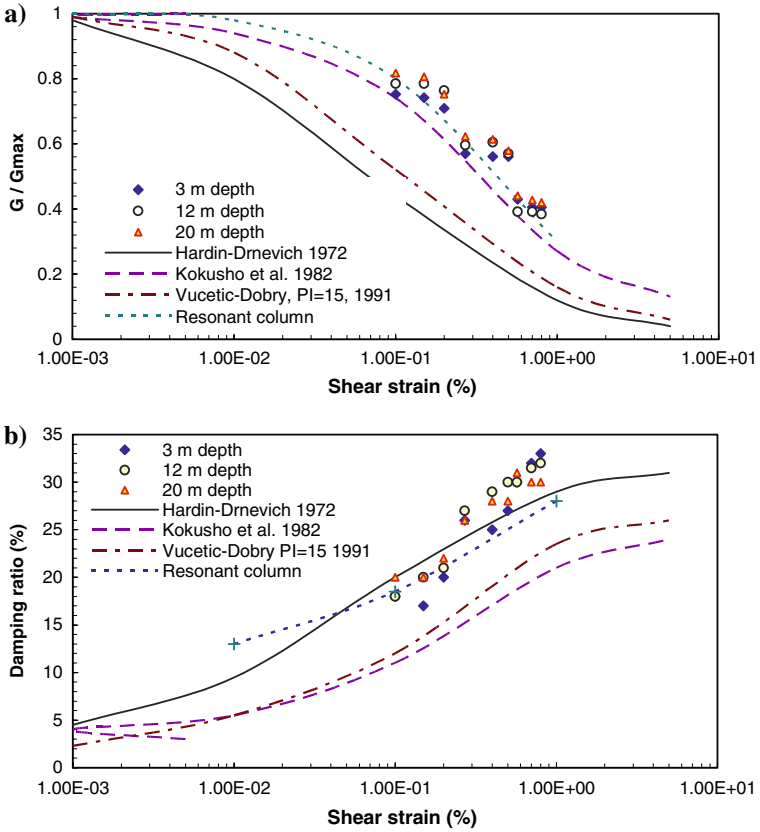

Fig. 5 (**a**) Shear modulus degradation and (**b**) damping ratio for soft clay, model RG-01

data, yielding modulus degradation curves. The damping ratio was calculated from selected stress–strain loops at 3 m, 12 m, and 20 m using the area of the actual shear stress–strain loop.

6.2.1 Shear modulus

Shear modulus values were derived from three accelerometers aligned vertically, i.e., A2 (20 m depth), A4 (12 m depth), and A6 (3 m depth) and were normalized by G_{max}. The shear modulus degradation curves at these locations are shown in Fig. 5a. The empirical relationships given by Hardin and Drnevich (1972), Vucetic and Dobry (1991), and Kokusho et al. (1982) are also plotted in Fig. 5a for comparison. The best fit curve of data obtained from resonant column tests on glyben clay with confinement pressure of 300 kPa is also included (Rayhani and El Naggar 2007).

The shear modulus ratio (G/G_{max}) obtained from the centrifuge tests decreased with the shear strain amplitude and increased with depth, indicating increase with confining pressure. As noted from Fig. 5a, they agree reasonably with the corresponding empirical relationships. The shear modulus at all shear strain range is remarkably close to the resonant column results and relationship proposed by Kokusho et al. (1982) for clay, while these data are higher than the design curves suggested by Hardin and Drnevich (1972) and Vucetic and Dobry (1991).

6.2.2 Damping ratio

Figure 5b presents the damping ratios estimated from the centrifuge test results, a best fit of the damping ratio of the resonant column tests (Rayhani and El Naggar 2007) and standard design curves proposed by Hardin and Drnevich (1972), Vucetic and Dobry (1991), and Kokusho et al. (1982). As expected, the damping ratio decreased with confining pressure, and increased with shear strain amplitude. The estimated centrifuge damping ratio is close to the empirical relations of Hardin and Drnevich (1972) and the resonant column results. However, for shear strain larger than 0.5% the damping ratio data is slightly higher than the corresponding Hardin and Drnevich empirical curves. The centrifuge data are noticeably far from the design curves suggested by Kokusho et al. (1982) and Vucetic and Dobry (1992) for fine grained soils. Such scatter in estimated damping values have been reported by Brennan et al. (2005) and Zeghal et al. (1995). Similar observations were also made by Elgamal et al. (2005).

6.3 Comparison of calculated and recorded responses

Site response analyses were performed using the program, FLAC (Fast Lagrangian Analysis of Continua) (Itasca 2005). A nonlinear analysis for the seismic ground response was performed and the results were compared with the recorded free field ground motion. The Mohr–Coulomb constitutive model was used to simulate the nonlinear soil behavior. The shear modulus and damping ratios estimated from the centrifuge data were used as input to these analyses. The shear wave velocity profile estimated from the T-bar test was used for the response analysis. The recorded time history at the base of the centrifuge container was used as the base input motion of the soil profile in the analyses. Calculated and recorded acceleration time histories and the corresponding response spectra in model RG-01 for the WCM earthquake are compared in Fig. 6. It is noted that calculated and recorded responses at all depths agreed well.

6.4 Amplification of input motion

Three accelerometers were located near the left side of the model and aligned vertically to study the amplification of free field motion and one accelerometer was located beneath the structure to investigate its effect on ground motion. Figure 7a depicts acceleration amplification with depth for all shaking events. The acceleration amplifications were obtained by normalizing the maximum recorded acceleration at a given elevation by the corresponding peak acceleration of the base excitation. Figure 7a shows that the soil stiffness and layering impacted greatly the characteristics of the ground motion through the soil profile. The acceleration of the free field was amplified, especially for low earthquake input motions. For model RG-01, the free field motion amplification varied between 1.5 during event WCL ($a_{\max} = 0.1g$) and 1.1 for event KH ($a_{\max} = 0.54g$). For RG-02, the amplification varied between 1.8 for event WCL and 1.1 for event KH. It is interesting to note that most of the amplification occurred in the upper soft layer, especially for low earthquake motions. This observation underscores the importance of considering the soil layering when evaluating the free field motion and not just the average of shear wave velocity in the top 30 m of the soil profile. This is also highlighted by the low amplification in the KH event, which is attributed to softening of the upper soft clay as the stress level increased.

Figure 7b shows the amplification at soil surface and beneath the structure for all shaking events. It is noted from Fig. 7b that the surface amplification was significant in low shaking

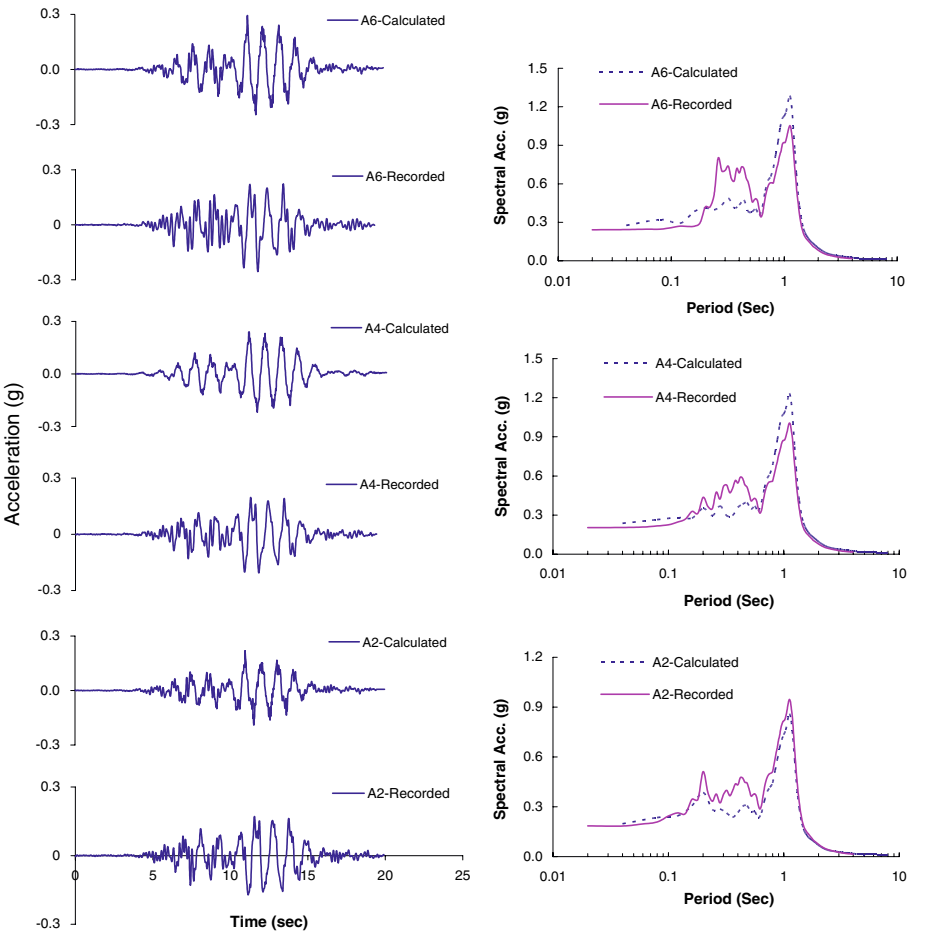

Fig. 6 Calculated and recorded acceleration time histories and response spectra in model RG-01 for event WCM (max $A = 0.2g$)

events, with larger amplification occurring for the layered soil profile. This is a further proof that the average shear wave velocity of the top 30 m is not a sufficient indicator for expected amplification as postulated in most seismic codes, including NBCC 2005. The soil layering should be carefully considered. The amplification factor decreased for stronger shaking events in both soil profiles. This reduction is because the soil experienced high stresses that approached its shear strength during strong shakings and probably caused failure thus limiting the stresses that can be transmitted to the upper soil layers. Furthermore, higher peak amplitude of the ground acceleration and strain levels in the soil is associated with higher material damping which further reduces the response.

The acceleration amplification beneath the structure was higher than that for the free field in model RG-01. The relative increase of acceleration beneath the structure was larger for stronger earthquake events which could be due to the structure feedback and strong interaction between the soil and foundation during shaking. For RG-02, the amplification factors for both free field and beneath the structure were similar. This is attributed to the presence of

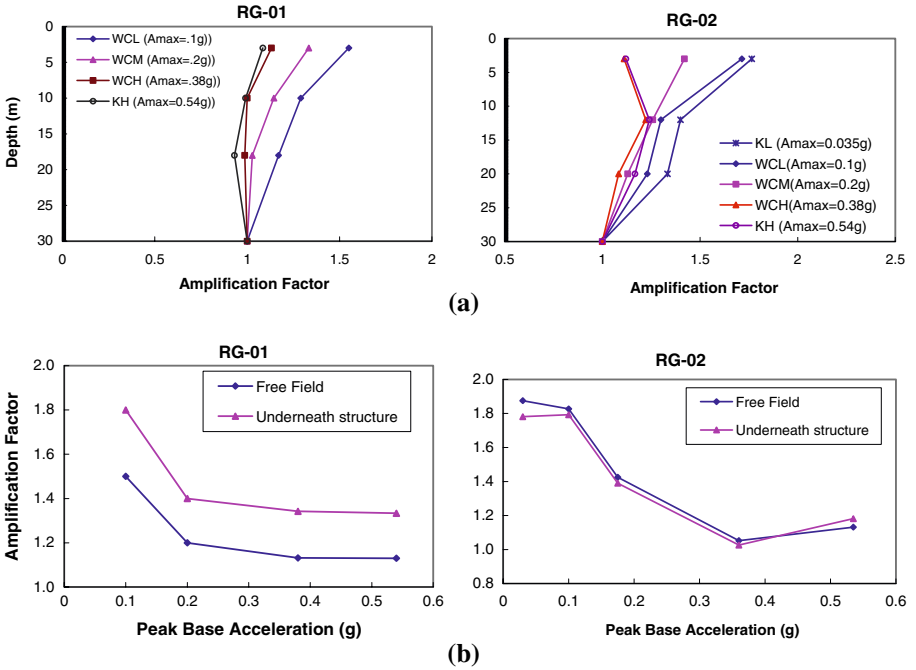

Fig. 7 (**a**) Variation of free field amplification factor with depth, and (**b**) Amplification of the free field and beneath the structure

a shallow softer soil layer with concentrated shear stresses beneath the structure, resulting in strong nonlinear behavior within this layer. The soil nonlinearity overshadowed the effects of the soil–structure interaction in this case.

6.5 Spectral analysis

Spectral analysis characterizes the frequency content of the strong input motion imposed on the structure and establishes the predominant frequency of the earthquake loading. In addition, the transfer function of the site can be established which can be used to assess the ground motion amplification and seismic hazard associated with different period earthquakes.

Figure 8 shows the acceleration response spectra of earthquake WCM ($a_{\max} = 0.2g$), with a damping ratio of 5%. It is noted that the acceleration response was amplified for most periods. The amplification was most significant during periods within the range 0.2–0.6 s, which shows the local site effects on the input motion. The spectral accelerations in model RG-01 varied between $0.8g$ and $1.1g$ for the free field and beneath the structure, respectively, and were about $1.0g$ for both free field and beneath the structure in RG-02. The peak accelerations beneath the structure in model RG-01 were somewhat higher than those at the free field suggesting strong interaction between the soil and the foundation in the period range of 0.3–0.5 s. However, for model RG-02, the peak acceleration beneath the structure was slightly less than those at the free field. As mentioned previously, this is attributed to the concentrated nonlinearity in the soft soil below the structure. The period of maximum response spectra were about 0.26 and 0.35 s for RG-01 and RG-02, respectively. The longer

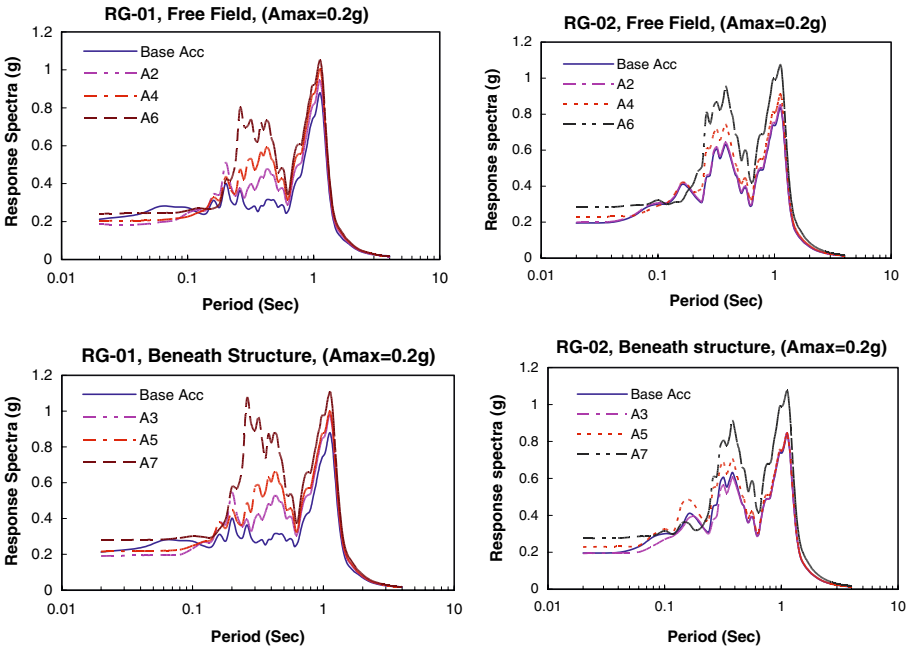

Fig. 8 Response spectra with peak base acceleration of $0.2g$

Table 7 Stiffness and natural period of the model structure

Model	Soil	Horozontal stiffness, K_u, (N/m)			Natural period (s)		
Event	description	WCL	WCM	WCH	WCL	WCM	WCH
RG-01	Uniform	1.23×10^8	1.1×10^8	5.9×10^7	0.29	0.31	0.41
RG-02	Layered	1.64×10^8	1.45×10^8	8.68×10^7	0.26	0.27	0.35

period in the case of RG-02 is attributed to the softening of the upper soft soil layer during strong excitation.

The relationship between the vibration periods of the model structure and supporting soil influences the seismic response of structures. The stiffness, K, and natural period of the model structure were estimated for both profiles and are shown in Table 7. It is noted from Fig. 8 and Table 7 that amplification has occurred close to the natural period of the model structure. The horizontal stiffness of the system decreased (i.e., period increased), due to shear modulus degradation with increasing the earthquake excitation.

Figure 9 shows the ratio of response spectra (RRS) curves defined as the acceleration response near the ground surface normalized by that of the base. The maximum values of RRS in RG-01 were about 3.0 and 3.8 for the free field and beneath the structure for WCH, and were about 1.9 for both in RG-02. It is noted that RRS for beneath the structure was higher than RRS for the free field, which shows strong soil–structure interaction in RG-01. The natural frequency of soil models RG-01 and RG-02 was 2.44 Hz and 2.86 Hz, respectively, for earthquake WCH. This provides a useful indication of the frequency of vibration

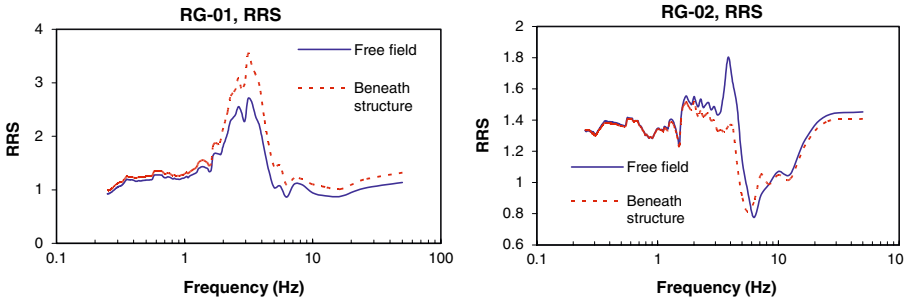

Fig. 9 Ratio of surface response spectra to base response spectra

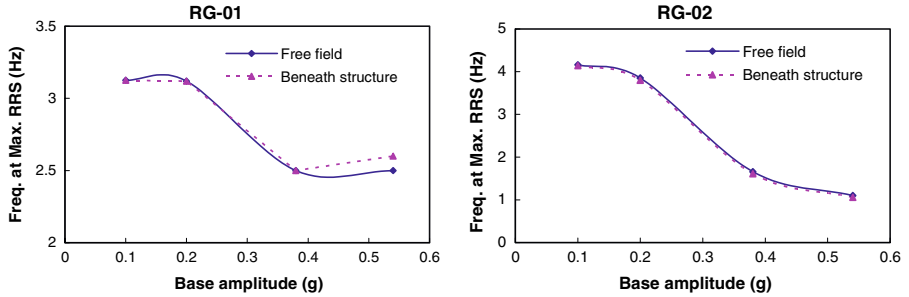

Fig. 10 Variation of natural frequency with shaking amplitude

at which the most significant amplification can be expected. The dynamic amplification has clearly occurred in the vicinity of the soil deposit natural frequency as can be seen in Fig. 9.

Figure 10 shows the variation of the peak RRS frequency with shaking amplitude for the free field and beneath the structure locations. The frequency at which maximum RRS occurred decreased with an increase in the earthquake intensity. This decrease could be due to a decrease in the soil shear modulus and increase in its damping ratio. The peak frequency for RG-01 decreased from 3.2 Hz to about 2.5 Hz. The decrease of peak frequency in RG-02 was more significant, i.e., from about 4 Hz (which compares well with the theoretical value) to about 1 Hz in stronger shaking events. This is attributed to significant nonlinearity within the weak upper layer of the layered profile.

6.6 Structural behavior

The spectral acceleration of A8 (adjacent to the structure) was compared with that of A14 (free field) in order to evaluate the interference of the structure with horizontal ground motion. Figure 11 shows that the response spectra near the structure were higher than free field acceleration at the same level, especially for periods close to the structure natural period (0.27–0.31 s), which indicates strong soil–structure interaction (SSI). The SSI was more pronounced for RG01. To further explore the effects of SSI, the ratios of accelerations A8/A14 and A7/A14 are compared in Fig. 12. Inspecting Fig. 12, it is noted that SSI resulted in amplifying the ground motion by 15–20% in RG-01. For RG-02, the SSI effects were much less, especially beneath the structure, which was attributed to the strong nonlinearity in the upper soft soil.

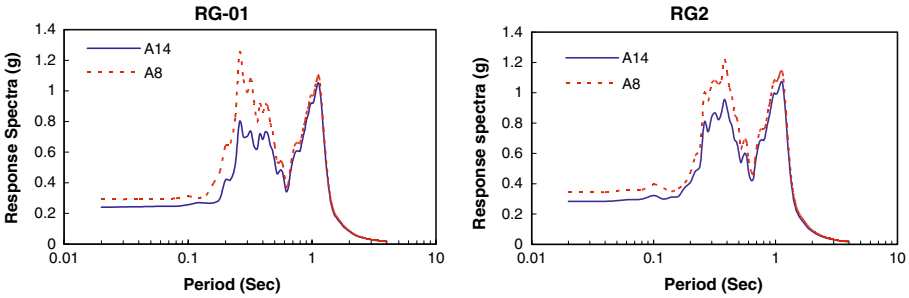

Fig. 11 Horizontal variation of response spectra on surface

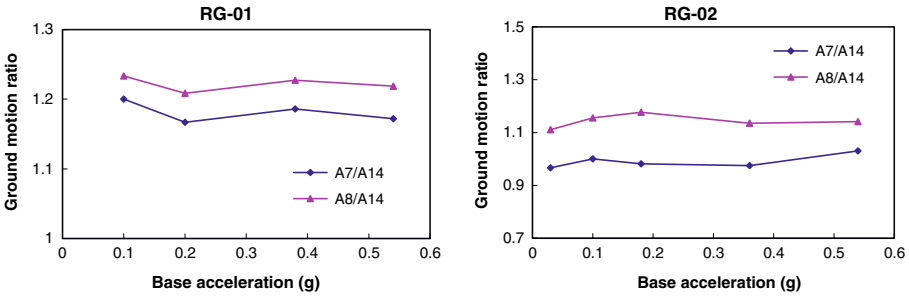

Fig. 12 Ground input motion ratio

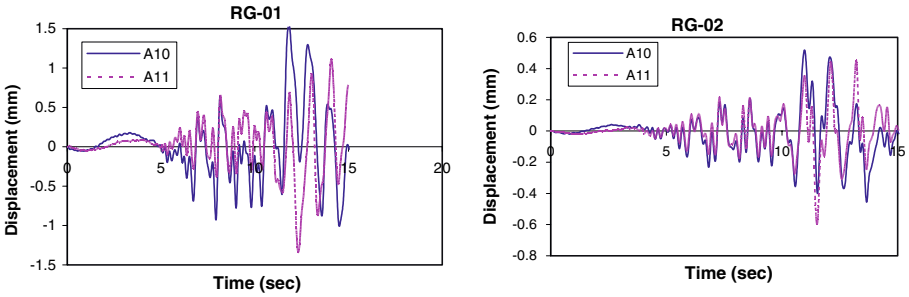

Fig. 13 Vertical displacement time history of two sides of structure

Vertical accelerometers A10 and A11 were attached along the top of structure to capture possible rocking behavior. Their displacement time histories, established by double integrating the acceleration time histories, are shown in Fig. 13. The time histories show similar movement trends for both sides of the structure and that there was no phase shift. It was deduced that the structure experienced negligible rocking in both models. In addition, a separation of less than one mm between the soil and the structure occurred during earthquake shaking (model RG-01).

Absolute displacements of different points were obtained by integrating the measured accelerations, and relative movement of different points could be obtained by subtracting their respective absolute displacements. The relative lateral displacement of the structure was estimated by subtracting its displacement (A12) from the displacement of the soil beneath it (A7). The maximum lateral displacement of the structure is plotted in Fig. 14 for all shaking

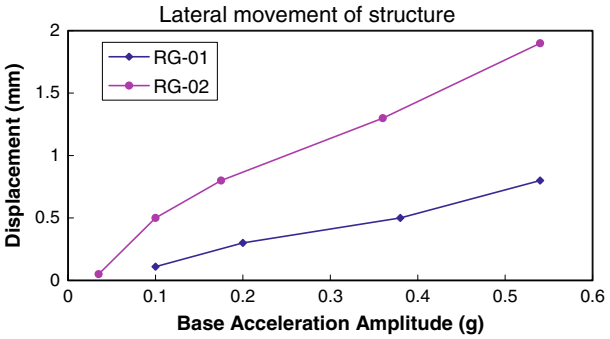

Fig. 14 Relative lateral movements of structure for all shaking events

events. The structure displacement increased with the level of shaking. For example, for the WCL event it was about 0.2–0.5 mm (prototype scale) for RG-01 and RG-02, respectively, and for the KH event the calculated values were 0.8 mm and 1.8 mm, respectively.

7 Summary and conclusions

A series of centrifuge model tests was conducted to study the seismic response of soft clay profiles and seismic soil–structure interaction. Several earthquake-like shaking events were applied to the model to investigate linear and nonlinear soil behavior.

Dynamic soil properties obtained from centrifuge test were in reasonable agreement with the empirical trends. The identified shear modulus reduction seemed to be relatively close to the empirical relations and in comparison with other published data in the literature. In addition, seismic site response analyses using a fully nonlinear procedure demonstrated the good agreement between the numerical simulations and centrifuge model recordings. These results confirmed the suitability of the glyben material as a soft soil model for centrifuge testing.

The amplification and the predominant frequency of the surface accelerations decreased with an increase in earthquake intensity. These effects were attributed to the reduction in soil stiffness and increase in its material damping as the earthquake amplitude increased. The acceleration amplification beneath the structure was higher than that for the free field in uniform soil, but was the same for the layered soil profile.

For the uniform soil, the peak accelerations of soil beneath the structure increased due to strong interaction between the soil and the foundation. In the case of the layered soil, however, the acceleration beneath the structure was slightly less than that at the free field. This was attributed to the strong nonlinearity within the weak soil layer beneath the structure. In addition, the decrease in the response frequency content during stronger earthquakes was more significant in the layered soil profile than for uniform clay. These observations clearly demonstrate that the layering system has to be considered, and not just the average shear wave velocity, when evaluating the local site effects. Finally, the obtained experimental data can be used to validate numerical models.

Acknowledgements The authors would like to thank Dr. Ryan Phillips, Director of C-CORE for his guidance and support during the centrifuge testing phase of this research as well as Gerry, Susan, Karl, Don Cameron, and Derry for their assistance in the centrifuge testing. Their help is gratefully acknowledged.

References

Bransby MF, Newson TA, Brunning P, Davies MCR (2001) Numerical and centrifuge modeling of the upheaval resistance of buried pipelines. In: Proceedings of OMAE pipeline symposium, Rio de Janeiro.

Brennan AJ, Thusyanthan NI, Madabhushi SPJ (2005) Evaluation of shear modulus and damping in dynamic centrifuge tests. J Geotech Geoenviron Eng ASCE 131(12):1488–1497

Coulter SE, Phillips R (2003) Simulating submarine slope instability initiation using centrifuge model testing. In: Paper ISSMM-062 1st international symposium on submarine mass movements and their consequences, EGS-AGU-EUG Joint Assembly Meeting, Nice. Kluwer Academic Publishers, The Netherlands

Elgamal A, Yang Z, Lai T, Kutter B, Wilson DW (2005) Dynamic response of saturated dense sand in laminated centrifuge container. J Geotech Geoenviron Eng ASCE 131(5):598–609

Hardin BO, Drnevich VP (1972) Shear modulus and damping in soil: design equations and curves. J Soil Mech Found Eng Div ASCE 98(7):667–692

Itasca (2005) FLAC Version 3.00, A computer program for seismic response analysis for soil deposits. Itasca Consulting Group, Inc., Minneapolis, MN, USA

Kenny MJ, Andrawes KZ (1997) The bearing capacity of footings on a sand layer overlying soft clay. Geotechnique 47(2):339–345

Kokusho T, Yoshida Y, Esashi Y (1982) Dynamic properties of soft clay for wide strain range. Soils Found 22(4):1–18

Lanzo G, Vucetic M, Doroudian M (1997) Reduction of shear modulus at small strains in simple shear. J Geotech Geoenviron Eng ASCE 123(11):1035–1042

Mayfield B (1963) The performance of a rigid wheel moving in a circular path through clay. University of Nottingham, PhD thesis

Randolph MF (2004) Characterisation of soft sediments for offshore applications. In: Viana da Fonseca, Mayne (eds) Proceedings ISC-2 on geotechnical and geophysical site characterization. Millpress, Rotterdam

Randolph MF, Houlsby GT (1984) The limiting pressure on a circular pile loaded laterally in cohesive soil. Geotechnique 34(4):613–623

Rayhani MT, El Naggar MH (2007) Characterization of glyben for seismic application. Geotech Testing J ASTM 31(1): Paper ID GTJ 100552

Seid-Karbasi M (2003) Input motion time histories for dynamic testing in the c-core centrifuge facilities. Report No. 2003/01, University of British Columbia

Tiers GR, Seed HB (1968) Cyclic stress–strain characteristics of clay. J Soil Mech Found Eng Div ASCE 94(2):555–569

Vucetic M, Dobry R (1991) Effect of soil plasticity on cyclic response. J Geotech Eng ASCE 117(1):89–107

Zeghal M, Elgamal AW, Tang HT, Stepp JC (1995) Lotung downhole array. II: evaluation of soil nonlinear properties. J Geotech Eng 121(4):363–378